



# Influence of nanoparticles and polymer branching on the dewetting of polymer films

Kathleen A. Barnes<sup>1</sup>, Jack F. Douglas<sup>2</sup>, Da-Wei Liu,  
Alamgir Karim\*

*Polymers Division, National Institute of Standards and Technology, 100 Bureau Dr., Stop 8542,  
Gaithersburg, MD 20899, USA*

---

## Abstract

Previous studies have shown that spun-cast films of unentangled synthetic polymers commonly dewet inorganic or organic substrates, leading to technologically detrimental results for many applications. We illustrate two strategies for influencing polymer film dewetting on inorganic and organic substrates. First, the addition of small amounts of C<sub>60</sub> fullerene nanoparticles to the spin-casting polymer solutions of model synthetic polymers [polystyrene (PS) and polybutadiene (PB)] leads to a significant inhibition of film dewetting on Si. This effect is associated with the formation of a diffuse fullerene layer near the solid substrate that frustrates the dewetting hole growth process. Next, we consider polymer branching effects on the dewetting of various generations of hypergraft polymer poly(2-ethyl-2-oxazoline) (PEOX) films cast on high molecular weight polystyrene substrates. The early stage of dewetting is found to be similar in a zeroth generation G0 hypergraft (a comb polymer) and a G2 hyper-graft (resembling a spherical ‘micro-gel’ particle). The late stage of dewetting in the G2 films, however, differs significantly from the low generation films because of an inhibition of hole coalescence in the intermediate stage of film dewetting. This behavior resembles previous observations of dewetting in ‘entangled’ polystyrene films. Thus, the viscoelasticity of the polymer film can have an inhibitory effect on film dewetting.

---

\* Corresponding author. Tel.: +1-301-975-6588; fax: +1-301-975-4924.

E-mail addresses: alamgir.karim@nist.gov (A. Karim), jack.douglas@nist.gov (J.F. Douglas).

<sup>1</sup>Current address: MS C043B1, Dow Corning Company, Midland, MI 48686-0994, USA.

<sup>2</sup>Corresponding co-author. Tel.: +1-301-975-6779; fax: +1-301-975-4924.

leading to changes in the dewetted film morphology rather than a suppression of film dewetting. © 2001 Elsevier Science B.V. All rights reserved.

*Keywords:* Nanoparticles; Polymer branching; Dewetting

---

## Contents

1. Introduction . . . . .	84
2. Experimental . . . . .	85
3. Results . . . . .	88
3.1. Suppression of dewetting in nanoparticle filled polymer films . . . . .	88
3.2. Influence of branching on the dewetting of polymer films . . . . .	95
4. Conclusion . . . . .	99
Acknowledgements . . . . .	102
References . . . . .	103

## 1. Introduction

Thin films are increasingly being used in technological applications involving dielectric coatings, resist layers for lithography, electronic packaging, optical coatings, non-linear optical devices, lubricating surfaces, etc. [1–3]. Producing stable and defect-free films is particularly problematic in very thin films (thickness,  $L < 10$  nm) where thermally-induced fluctuations of the polymer-air film boundary ('capillary waves') tend to cause film rupture [4–10]. The wettability of polymers on surfaces is important in producing stable organic polymer films on inorganic substrates. Stabilization of these films against dewetting is a problem of fundamental technological importance.

Various strategies have been utilized to 'stabilize' thin polymer films. Dewetting can be greatly suppressed in high molecular weight (entangled) or glassy polymer films ( $T < T_g$ ) spun cast from solution. It is difficult for these films to equilibrate so that surface energy is less of a factor governing film stability. In practice, polymer films are often 'stabilized' by preparing them out of equilibrium in a glassy or entangled state. The stabilization is kinetic because no dewetting occurs over very long timescales under controlled conditions. Under more variable conditions, the 'aging' of the film structure and associated formation of film defects over time can be detrimental to the applications for which the films were intended. Recent work has also shown that the tendency towards polymer film dewetting on inorganic substrates can be inhibited through grafting polymer layers onto the solid substrate with and without the addition of high molecular weight polymer [11], sulfonation and metal complexation of the polymer [12] and the introduction of specialized end-groups onto the polymer with a high affinity for the inorganic

substrate [13]. At present, these film stabilization effects are not well understood theoretically, but it seems clear that a combination of equilibrium (modification of polymer-surface interactions) and kinetic stabilization effects (entanglement and changes in  $T_g$ ) are generally involved [14–16].

In the present paper, we consider two strategies to inhibit the dewetting of thin polymer films. First, we take the novel approach of introducing  $C_{60}$  fullerene nano-particles to the spin-casting polymer solution. This film stabilization effect is contrary to the usual experience where film inhomogeneities are found to lead to ‘cratering’ (hole formation) in thin films [17,18]. Stange et al. [19] and Jacobs et al. [20] have recently emphasized the importance of small particulates and air bubbles in nucleating the formation of holes in polymer films so there is evidence that film heterogeneities can have a detrimental effect on film stability. The nanoparticle fillers correspond to a very different size scale, however, and it is not immediately clear what influence such heterogeneities would have on the stability of polymer films. We show that the addition of even a very small amount (mass fraction,  $\phi_{\text{filler}} = 0.01\%$ ) of fullerene (or ‘buckyballs’, BB) particles to the spin-casting solution leads to a strong inhibition of film dewetting for polystyrene and polybutadiene films in a thickness range between 20 and 50 nm. The films were cast on acid-cleaned silicon wafers. Control measurements for unfilled films having nearly the same thickness indicated a pattern of dewetting for this thickness regime that is initiated by hole formation and growth at early stages and patterned droplets at late stages.

To gain some insight into the influence of chain branching we decided to study hyperbranched polymer films having a range of ‘branching intensity’. We contrast the dewetting of model polymer films from model generation G0 and G2 hypergraft polyethyloxazoline (PEOX) films. The viscoelastic properties of PS hypergraft polymers having a similar topology have previously been shown to have significant changes in their viscoelastic properties with generation number [21]. The G0 hypergraft PS polymers are found to have properties similar to unentangled linear or lightly branched (combs, few arm stars) polymers while the G3 PS hypergraft formed a gel-like material at room temperature [21]. The G2 PS hypergraft remains a liquid and has an extended plateau in its shear stress relaxation that is reminiscent [21] of entangled linear polymers [22] or micro-gel particles [23,24]. Thus, the G2 PEOX hyperbranched polymers of the present study can be expected to exhibit the flow properties of a highly viscoelastic fluid and below we compare the dewetting properties of the G2 fluid to modestly entangled linear polymer fluids. The substrates were a highly viscous polymer layer (entangled PS) that did not dewet from its silica underlayer on the timescales of our measurements and the hyperbranched polymers were also spun-cast directly onto acid-cleaned silica wafers.

## 2. Experimental

In our studies of nanofiller-induced film stabilization we utilized low molecular

weight polystyrene (PS) and polybutadiene (PB) samples from Goodyear Tire and Rubber Company<sup>3</sup>. These polymers have reported average molecular masses<sup>4</sup> and polydispersity values of  $M_n = 1800$ ,  $M_w/M_n = 1.19$  and  $M_n = 2760$ ,  $M_w/M_n = 1.08$ , respectively. The glass transition temperature ( $T_g$ ) of pure PS was determined by differential scanning calorimetry (DSC) to be  $55 \pm 2^\circ\text{C}$  while the  $T_g$  of PB is estimated to be  $< -50^\circ\text{C}$ . PS was purified upon receipt by filtration followed by freeze-drying.  $C_{60}$  fullerenes ('buckyballs', BB)<sup>2</sup> were purchased from Aldrich Chemical Company and dissolved in toluene before addition to the polymer solutions. The fullerene particles readily dissolved into the spin-casting polymer solutions where the fullerene mass fractions were in the range (0.01 to 5%) in PS and 1% in PB. The polymer-fullerene mixtures and the spin-casting solutions containing fullerene were optically transparent and had a light violet color, as often found for fullerene solutions in organic solvents. Spin casting solutions were all prepared in toluene and were spun cast at various speeds ranging from 2000 to 6000 rev./min (rpm) to obtain films ranging from 20 to 50-nm thick<sup>5</sup>. Polymer/toluene solutions were filtered through 0.2- $\mu\text{m}$  PTFE filters before spin-coating. (It is difficult to determine the exact fullerene concentration of the spun cast films since the concentration ratio of polymer to filler may not be maintained during spin-casting because filler adsorption and other non-equilibrium effects associated with spin-coating process). The silicon wafer substrates were acid cleaned with a 70:30 volume ratio solution of 96%  $\text{H}_2\text{SO}_4$ /30%  $\text{H}_2\text{O}_2$  for 1 h at  $80^\circ\text{C}$  and rinsed in deionized water before spin-coating. Films were also spun onto Si wafers uniformly coated with freshly evaporated carbon ( $\approx 100\text{-nm}$  thick) under high vacuum.

Small angle neutron scattering (SANS) measurements on filled bulk PS samples containing up to 1% fullerene mass fraction do not show evidence for a  $q^{-4}$  power law scaling or other power law scaling which would be symptomatic of the aggregation of fullerene particles into compact or fractal clusters, respectively. Clustering would be apparent even at low fullerene concentrations because of the high contrast between the fullerene and the polymer solution. Given this lack of aggregation, at least for these low concentrations of filler, we expect the relative filler concentration in the dried film to be proportional to the filler concentration

---

<sup>3</sup>Certain commercial equipment, instruments, and materials are identified in this article in order to adequately specify experimental procedure. Such identification does not imply recommendation or endorsement by NIST, nor does it imply that the materials or equipment identified are necessarily the best available for the purpose.

<sup>4</sup>According to ISO 31-8, the term 'molecular weight ( $M_w$ )' has been replaced with 'relative molecular mass', symbol  $M_{r,w}$ . The conventional notation, rather than the ISO notation, has been employed for this article.

<sup>5</sup>It is difficult to determine if the concentration of filler in the spun-cast film layer is the same as the casting solution since an undetermined amount of filler may wash off during spin-casting. The neutron reflectivity fits were not sensitive to fullerene concentration in the film for a mass fraction of 5%. Filler concentration in the paper therefore refers to that in the casting solution, e.g.  $\phi_{\text{filler}} = 0.01$  refers to the filler mass fraction relative to the polymer mass in solution.

in the spin-casting solution. Fullerene particle aggregation cannot be excluded in the dried film (see Section 4), however.

Optical microscopy (OM) indicated that the PS films were smooth and uniform when inspected immediately after spin coating. The films were annealed under vacuum at 45 and 85°C above the glass transition of the PS ( $T = 100$  and 140°C, respectively) to observe the dewetting process. Since the glass transition of PB is well below room temperature, annealing at higher temperatures was not necessary to induce dewetting. Reflective optical images were obtained using a Nikon optical microscope<sup>2</sup> with a digital Kodak MegaPlus CCD camera attachment<sup>2</sup>. Atomic force microscopy (AFM) images of the surface patterns were taken using an Explorer TopoMetrix instrument<sup>2</sup>. Contact angle measurements were estimated by dropping 5  $\mu\text{l}$  of deionized water on the film surface with values averaged from four droplet readings using a Rame–Hart contact angle goniometer<sup>2</sup>. Glass transition temperatures of filled and unfilled PS films were measured using a Perkin-Elmer differential scanning calorimeter (DSC)<sup>2</sup>.

Neutron reflection [25] (NR) measurements were performed on a thin PS film containing a fullerene mass fraction of 5%, prepared on polished acid cleaned Si wafers (diameter = 100 mm, thickness = 5 mm) using the cleaning procedure described above. The film was prepared by spin-casting a solution from toluene containing a total solid (PS and fullerene) mass fraction of 2% at 2000 rev./min to prepare a film approximately 100 nm thick. NR measurements were conducted on the NG7 reflectometer at the NIST Center for Neutron Research (NCNR). At NG7, neutrons of wavelength  $\lambda \cong 4.8 \text{ \AA}$  were collimated and reflected from the horizontally placed sample and the reflected beam monitored by a shielded He [3] pencil detector. The desired neutron momentum ( $q$ ) range was attained by changing the angle of incidence  $\theta$  while keeping the detector at  $2\theta$  position with respect to the incident beam.

In our studies of branching effects on film dewetting we employed thin films of deuterated PS [poly(styrene- $d_8$ , Polymer Laboratories<sup>2</sup>)] with a reported mass<sup>2</sup>,  $M_w = 188\,000 \text{ g/mol}$ , polydispersity,  $M_w/M_n = 1.05$ . The polymer films were spun-cast from toluene solutions at a polymer mass fraction of 1% at 1000 rev./min onto acid-cleaned silica substrates and annealed under vacuum at 130°C for 30 min to remove any residual solvent in the film. The entanglement molecular mass of PS equals [26,27]  $M_e = 1.8 \times 10^4$  so that the substrate polymer films are highly entangled. The silica wafer substrates were previously cleaned in a solution with 70% volume fraction concentrated sulfuric acid and 30% volume fraction hydrogen peroxide at 80°C for 1 h, followed by rinsing in deionized water and drying under nitrogen gas. Hypergraft and linear poly(2-ethyl-2-oxazoline) (PEOX) solutions (generations G0 and G2, respectively [28]), having a 1% mass fraction in methanol were spun cast at 2000 rev./min onto the PS coated silica or onto bare acid-cleaned silica substrates. The films were then imaged as cast after annealing under vacuum for a range of time intervals. Reflection optical microscopy images were taken using a Nikon microscope<sup>2</sup>. The PEOX hypergraft polymers (sometimes termed ‘dendrigrift’ polymers) were obtained from Michigan Molecular Institute<sup>2</sup> and their synthesis was previously reported [28]. The samples studied

were a linear PEOX polymer with  $M_w = 30\,000$  and dendrigrafts in the series  $[100_x - 100]$  with  $x = 1$  and 3 where 100 denotes the degree of polymerization of backbone and the grafts [28]. The  $x$  designation refers to G1 in the present work. Properties of topologically similar PS hypergraft polymers for generations 0, 1, 2 and 3 have recently been described by Gauthier and co-workers [29] and PS hyperbranched molecules in monomolecular films have been directly imaged by atomic force microscopy [30]. We expect that the PEOX hypergraft molecules to have a similar structure to the PS hypergrafts. Characterization of the PEOX hypergraft polymers is described in [28].

### 3. Results

#### 3.1. Suppression of dewetting in nanoparticle filled polymer films

Fig. 1a,b shows optical micrograph images from 50-nm thick films of pure PS and PS with fullerene mass fraction of 1%, respectively. Both films were annealed identically at 140°C for 20 min. This comparison indicates that the filled polymer film is ‘stabilized’ against dewetting on this time scale by the presence of the fullerene particles. The insets of Fig. 1a,b shows that the polymer films are uniform and homogeneous immediately after spin coating. Once annealed above the bulk glass transition of PS ( $T_g \approx 55^\circ\text{C}$ ), the pure PS polymer exhibits a typical pattern of dewetting initiated by nucleated holes at early stage as in Fig. 1a, followed by hole growth and coalescence [4,5]. In contrast, the 1%-filled PS film remained smooth on the spatial scales probed by the optical measurements. Since it is unclear whether the inhibition of film dewetting is a kinetic or equilibrium effect we annealed a representative 1% fullerene film over a 48-h period. Optical measurements indicated that the film remained smooth over this time period. This preliminary measurement indicates that either the fullerene brings about an equilibrium stabilization or a long term kinetic inhibition of film dewetting. In any event, the film dewetting process is inhibited over appreciable time scales and we next focus on the generality of the effect and try to understand its cause.

We can gain some insight into the generality of the film stabilization effect by considering the influence of the fullerene filler on the dewetting of another model polymer. An elastomeric polymer, polybutadiene (PB) provides a good contrast to the glassy PS polymer, both in its mechanical properties as well as in differences of surface energy [3]. Fig. 2a shows an optical micrograph of a PB film dewetting from the silicon substrate measured 5 min after spin coating. The film is approximately the same thickness ( $\approx 50$  nm) as the PS films shown in Fig. 1. Since room temperature is well above the  $T_g$  of PB, dewetting occurs rapidly giving rise to classic late-stage patterned droplets shown in Fig. 2a. The dewetting of the filled PB film ( $\phi_{\text{filler}} = 0.01$ ) in Fig. 2b is contrasted with the unfilled PB film of Fig. 2a of similar thickness ( $\approx 50$  nm). By comparison, the filled film was stable against large scale dewetting for a period greater than 8 h. Film stabilization by the nanofiller then occurs for both PS and PB filled films ( $\phi_{\text{filler}} = 0.01$ ,  $L \approx 50$  nm).

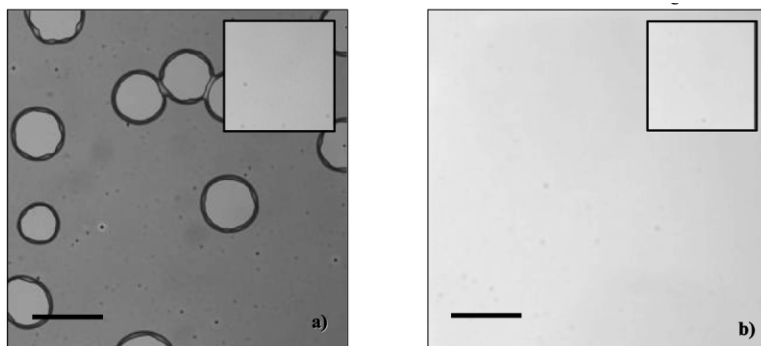


Fig. 1. Optical micrographs showing dewetting of 50 nm polystyrene films prepared by spin-casting polymer solutions onto acid cleaned silicon wafers after annealing at 140°C for 20 min. (a) PS, (b) PS with fullerenes ( $\phi_{\text{filler}} = 0.01$  in toluene). Insets show films prior to annealing (scale bar = 300  $\mu\text{m}$ , same for insets).

We next consider the influence of the film thickness and fullerene concentration on the suppression of film dewetting by the filler. Fig. 3a shows a thinner PS film ( $L \approx 20$  nm) that was annealed at 100°C for 30 min. The dewetting characteristics are roughly comparable to a film of this thickness [7,8]. In contrast, a 20-nm-filled PS film with a small concentration of fullerene ( $\phi_{\text{filler}} = 0.005$ ) showed no appreciable dewetting after 30 min of annealing at 100°C. Optical microscopy measurements performed after further annealing at elevated temperatures (140°C for approx. 3 h) did not provide any indications of dewetting (Fig. 3b), which is interesting given the very low concentration of filler employed in these measurements. Here we note that while the dewetting mechanism in the 50 and 20 nm films may be different (heterogeneous or in cross-over regime for 50 nm while spinodal-

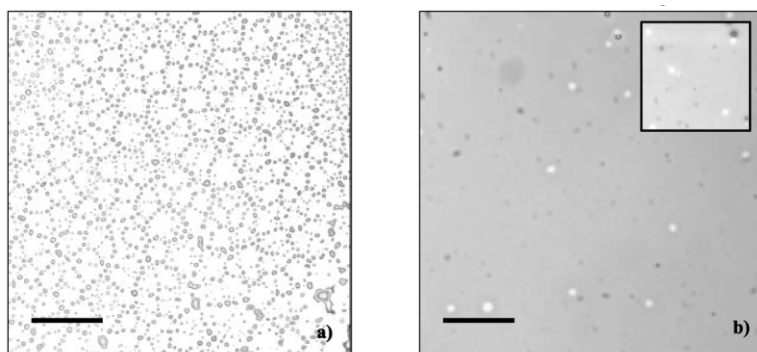


Fig. 2. Optical annealing showing dewetting of 50 nm polybutadiene films 5 min after spin-casting polymer onto acid cleaned silicon wafers. (a) PB, (B) PB with fullerenes ( $\phi_{\text{filler}} = 0.01$  in toluene). Inset of Fig. 2b shows the same film after 8 h (scale bar = 300  $\mu\text{m}$ , same for insets).

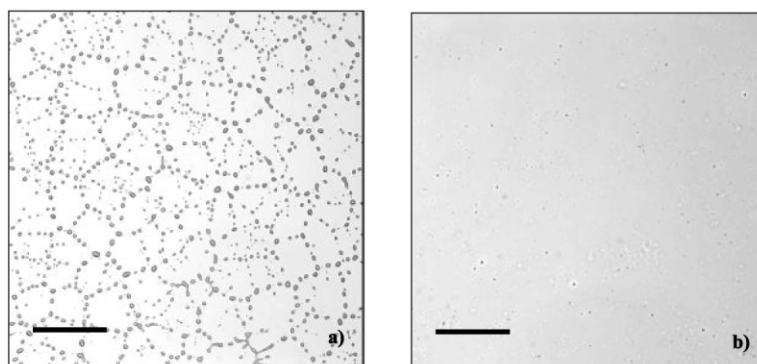


Fig. 3. Optical micrographs showing dewetting of 20 nm polystyrene films (a) PS annealed at 100°C for 30 min, (b) PS with fullerene mass fraction,  $\phi_{\text{filler}} = 0.005$  in toluene, annealed at 100°C for 30 min and then further annealed at 140°C for 2.5 h (scale bar = 300  $\mu\text{m}$ ).

like for the 20 nm film [7]), the suppression effect by the addition of fullerenes is apparently a general effect.

The films were then examined at a much higher magnification using AFM to determine if we were missing any important fine structure in the filled polymer films that might give us a clue into the origin of the film stabilization effect. Fig. 4a shows AFM of the same 20 nm dewetted film imaged in Fig. 3a (annealed for 30 min at 100°C). The droplets in this figure have a height on the order of 100 nm and the dark background indicates the bare dewetted silicon substrate. Fig. 4a provides a reference point for comparison to the fullerene filled polymer film prepared to have a similar film thickness and annealing history. We next contrast the relatively smooth looking optical image of the filled PS film shown in Fig. 3b ( $L \approx 20$  nm, annealed for 30 min at 100°C and 3 h at 140°C) with its AFM image shown in Fig. 4b. Interestingly, the dewetting of this filled polymer film with a very low filler concentration occurs only at a scale resolvable by our AFM. This image suggested to us that the growth of dewetting regions is arrested by the pinning of the contact lines of the growing holes. Such a pinning mechanism could arise from an inhomogeneous distribution of nanofiller bound to the substrate. This would also lead to a broad distribution of hole sizes as observed in Fig. 4b. It is notable that both the AFM (not shown) and optical images (see Fig. 1b) of PS films having a higher filler concentration (e.g.  $\phi_{\text{filler}} = 0.01$ ) show no evidence of hole formation so that the observation of holes is limited to low filler concentrations. Although the films having a low filler concentration have a more limited effect on achieving film stabilization against dewetting, they are helpful for understanding the origin of the film stabilization effect.

We can obtain further insight into the ‘pinning’ of the hole growth by examining more closely the early stages of dewetting in unfilled films where hole formation dominates the film dewetting process. The contrast between the filled and unfilled

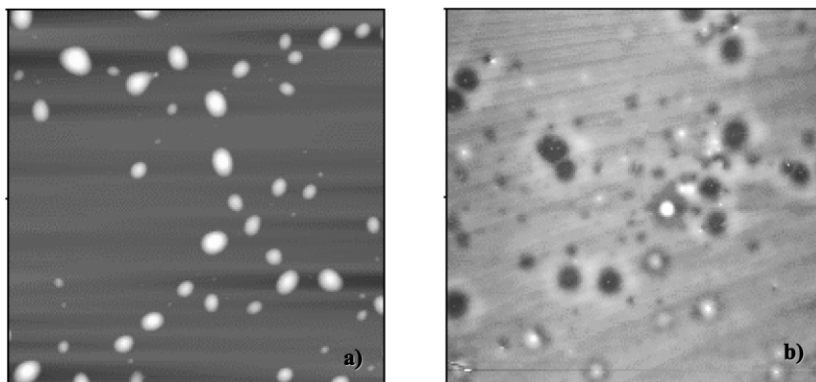


Fig. 4. AFM images of PS films with and without nanofiller (fullerene) particles. Images correspond to the same films whose optical micrographs are shown in Fig. 3, but at a higher spatial resolution. Film thickness are estimated to be 20 nm (a) PS annealed at 100°C for 30 min, (b) PS with fullerene mass fraction,  $\phi_{\text{filler}} = 0.005$  in toluene, annealed at 100°C for 30 min (almost no dewetting observed) and then further annealed at 140°C for 2.5 h. Note the height scale bar in Fig. 4b is 1/16 that in Fig. 4a, so the absolute heights in the filled film are significantly smaller compared to the unfilled dewetted film.

films is particularly apparent in these earlier stages of film dewetting. Fig. 5 shows a representative AFM image of hole formation in an unfilled PS film ( $\approx 35$  nm) that was obtained in a previous study of thin polymer film dewetting [7,8]. The polymer molecular weight in this former study was higher so the kinetics is slower, even at a higher temperature. This image is representative of hole formation in the early stage of dewetting in unfilled films (see also [4,5] for further examples). The hole size and shape is more uniform compared to the filled polymer films (Fig. 4b) that is characteristic of film dewetting without filler (Fig. 5). The kinetics of hole growth is even more distinctive between the filled and unfilled films. Holes that form in the unfilled film grow steadily in time and undergo a complex coalescence kinetics at a late stage of dewetting [4,5,7,8], while the holes of the unfilled film become pinned at a scale corresponding to the early stage of dewetting without filler. After pinning, the film structure shows no detectable evolution on the timescales of our measurements (8 h). The time scale of this pinning process is discussed below in connection with the influence of filler concentration on the size of the pinned holes.

It is well known that the evaporation of solvent from fullerene suspension in non-polar solvents such as toluene results in the formation of fractal dendritic structures. Clustering of the fullerene was also anticipated in polymer-fullerene films cast from non-polar solvents [31]. We checked for the presence of a layer of enriched filler concentration at the solid substrate through neutron reflection (NR) measurements. These measurements had a depth resolution of approximately 1 nm for a PS film of moderate thickness,  $L \approx 100$  nm and a relatively high filler concentration ( $\phi_{\text{filler}} = 0.05$ ) was employed to enhance sensitivity of our NR measurements. The solid line fit to the reflectivity data in Fig. 6 and the inset

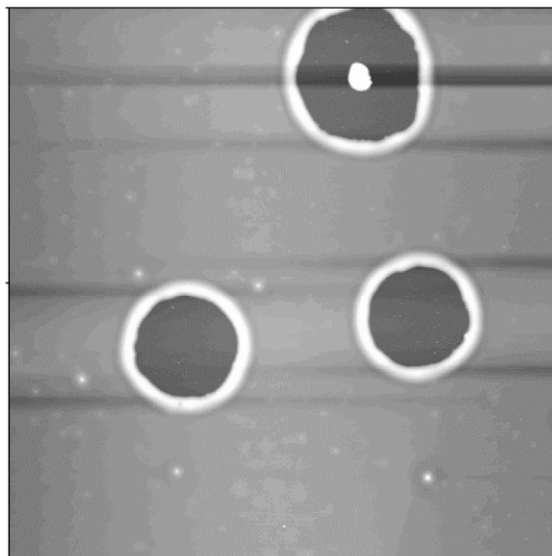


Fig. 5. AFM image of an unfilled 35-nm-thick PS film ( $M_w = 4000$ ) [7,8] dewetting from an acid cleaned silicon wafer after annealed for 25 h at 115°C. The top hole may be induced by a nucleating site such as dust. The holes are comparatively more uniform than that found in filled films.

shows the relative fullerene concentration or ‘composition profile’. The fullerene particles indeed form an approximately  $5 \pm 0.5$ -nm thick layer of enriched concentration near the silicon substrate. This enrichment apparently forms because the fullerene–silicon substrate interaction is apparently less unfavorable than the PS–silicon substrate interaction (PB enriches to the silicon substrate in PS/PB blends for a similar reason). The extent of this layer, however, is almost certainly influenced by the non-equilibrium conditions of the film casting process. The interface of the fullerene enrichment layer is diffuse relative to a monolayer of fullerenes, as expected based on previous observations showing the tendency of fullerene particles to form fractal dendritic structures on the solid substrate of evaporating films [31]. We anticipate that the roughness of the polymer–fullerene interface is greater in the cast films containing lower concentrations of fullerene because the substrate should only become completely covered at higher filler concentrations. It is difficult to characterize the in-plane structure of the polymer–fullerene interface using NR, but it may be possible to use grazing incidence X-ray scattering or other methods (e.g. secondary ion mass spectroscopy<sup>6</sup> to obtain information about the in-plane heterogeneity of the surface layer of fullerene enrichment [32]. NR data also indicates that there is no detectable enrichment of

<sup>6</sup>Average hole sizes were determined by measuring a minimum of 20 randomly selected holes for each optical image. Error estimations are based upon three average hole size calculations obtained from independent measurements.

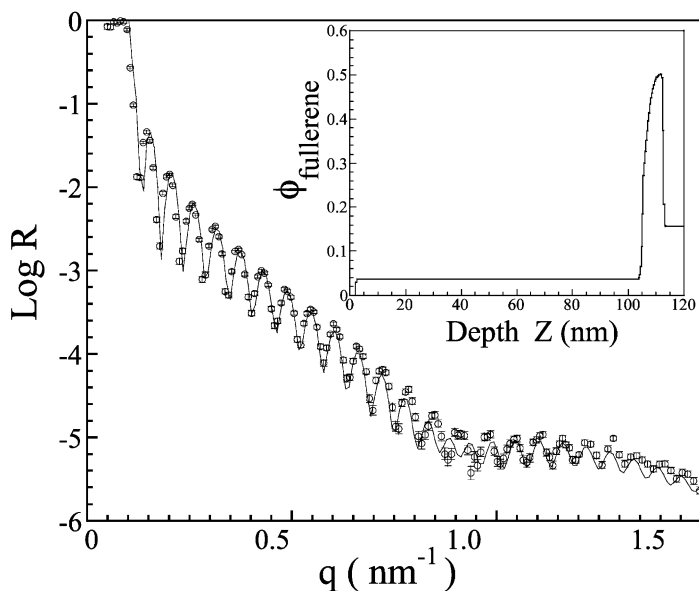


Fig. 6. Neutron reflectivity from a 100-nm-thick PS film containing fullerenes,  $\phi_{\text{filler}} = 0.05$ . Inset shows the volume fraction profile for the fullerene concentration in the film. Observe the fullerene segregated layer ( $\approx 5$  nm) at the silicon boundary with no detectable segregation at the air-polymer surface. The interface between the fullerene segregated layer and the PS film is diffuse. Error bars on data represent 1 S.D.

the fullerene particles at the polymer-air interface so that mechanisms of suppressed dewetting relying on the segregation of the fullerene to the polymer-air interface can be excluded.

Indirect information about the heterogeneity of the fullerene layer can be determined by varying the fullerene concentration and thus the fractional coverage of the solid substrate by the fullerene particles. According to our view of the suppressed dewetting due to contact line pinning, dewetting should occur within surface regions free of fullerene and become arrested when the contact line of the growing holes impinge on surrounding rough fullerene-rich regions of the substrate. This conceptual model should lead to a dependence of the average hole size on the filler concentration, hole sizes that are polydisperse because of the fluctuations in the surface coverage by the fullerene and most importantly, the hole growth is predicted to ‘pin’ at long times in this model. The average scale of the dewetting holes diminishes with an increasing filler concentration where the precise decrease depends on the particular geometrical form of the fullerene particle clustering on the substrate. To test the prediction of a decrease of hole size with increasing concentration in nanoparticle filled films, we made a series of filled PS films ( $L \approx 50$  nm) having a concentration range with mass fraction,  $0.0001 < \phi_{\text{filler}} < 0.05$  in the spin-casting solution. As shown in Fig. 7, the optical microscopy

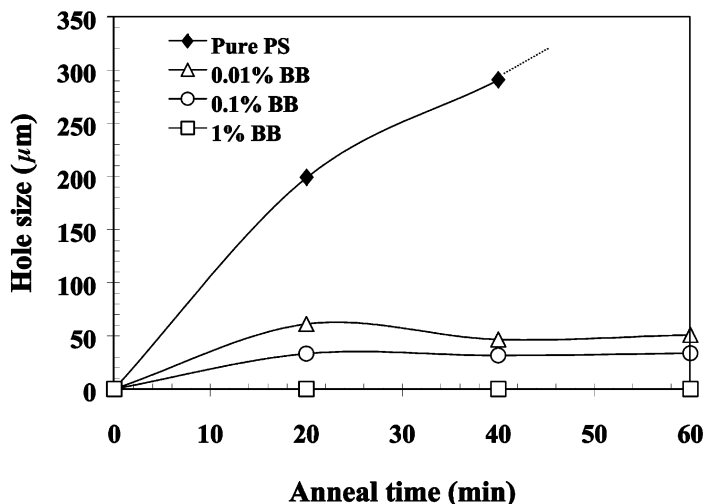


Fig. 7. Dewetting hole size in PS films ( $L = 50$  nm) as a function of fullerene filler mass fraction and annealing time at  $140^{\circ}\text{C}$ . The pure PS film shows approximately  $200\ \mu\text{m}$  hole growth by 20 min that start to impinge upon one another at longer times. The holes in the fullerene filled films do not grow ('pinned') beyond the first 20 min of annealing (The lines are simply guides for the eye and the overshoot for 0.01% BB at 20 min is an artifact of sampling error).

images indicate that the hole growth became pinned after 20 min of annealing at  $140^{\circ}\text{C}$  in all cases. Calculation<sup>5</sup> of the average hole size was determined by measuring the diameter of holes, giving average hole diameters at 20 min of  $50.8\ \mu\text{m} \pm 1.1\ \mu\text{m}$  and  $32.7 \pm 0.8\ \mu\text{m}$  for the  $\phi_{\text{filler}} = 0.0001$  and  $\phi_{\text{filler}} = 0.001$  films, respectively. The hole size did not evolve in time confirming also that the holes are 'pinned'. Both optical and atomic force microscopy indicated the absence of detectable holes for the films having  $\phi_{\text{filler}} = 0.01$  and  $\phi_{\text{filler}} = 0.05$  so that there appears to be a critical filler coverage beyond which hole formation becomes suppressed even in AFM measurements. Fig. 1b shows an optical image of the  $\phi_{\text{filler}} = 0.01$  concentration film after annealing at  $140^{\circ}\text{C}$  for 20 min. It is noted that by comparison that the average hole size of the unfilled PS film under the same annealing conditions and film thickness ( $L \approx 50$  nm) was  $200 \pm 12\ \mu\text{m}$  after 20 min and the holes are still growing. These observations confirm that the scale at which the dewetting holes pin diminishes with filler concentration and support our interpretation of the suppressed dewetting in terms of contact line pinning induced by a rough layer of adsorbed filler particles.

The presence of a fullerene layer at the air-polymer interface could dampen the capillary waves that are the likely source of instability causing the dewetting. To further confirm the lack of significant segregation of the fullerene to the air-polymer interface indicated by NR, we characterized the polymer-air surface energy through contact angle measurements. Table 1 shows results of water contact angle measurements on the filled and unfilled polymer films. Contact angle measure-

ments between all PS/fullerene surfaces and deionized water yielded angles of  $\approx 90^\circ$ , so that the surface energy seems to be relatively unchanged from that of pure PS films. A contact angle of approximately  $70^\circ$  was observed for deionized water droplets on the evaporated carbon films and the same value was found for spun-cast fullerene layers. These observations are consistent with our hypothesis that the fullerene and carbon layers should have similar surface energies. These measurements do not exclude the possibility that the rough nature of the fullerene layer changes the effective surface interaction substantially from the case of a smooth surface, leading perhaps to an equilibrium film stabilization effect in the filled polymer films. Large changes in the surface energy of films due to surface roughness have been observed [33] so that the inhibition of film dewetting due to fullerene and other nanoparticles is likely due to a combination of kinetic and equilibrium effects.

### 3.2. Influence of branching on the dewetting of polymer films

Fig. 8 shows the dewetting for a G0 PEOX film at a late stage of dewetting ( $t = 25$  min,  $T = 135^\circ\text{C}$ ) from a viscous polystyrene substrate. This dewetting morphology is typical of previous studies [34] of low molecular weight ('unentangled') polymer films dewetting for this range of film thickness, so we do not discuss this case further. This 'normal' dewetting scenario should be kept in mind when we compare with the dewetting of highly branched (G2) polymer films from the same substrate.

The as-cast film G2 PEOX film is smooth and circular holes form at random positions within the plane of the film. (Image not shown because of the similarity to many previously published images of early stage film dewetting [34]). The initial stage of the dewetting process is then remarkably similar to the observations on unentangled linear and G0 films [34]. However, as the holes of the entangled polymer films grow to sufficient size to impinge on each other, we see a striking change in the dewetting dynamics. In the G2 polymer film the holes press against each other, but do not seem to coalesce. A similar behavior has been observed in entangled linear chain polymer films whose molecular weight is not so high as to prevent dewetting [35]. In Figs. 9 and 10 we see direct evidence for the hole growth in time and the tendency to become distorted as they press against each other

Table 1

Average contact angles obtained by measuring the contact angle of  $5\ \mu\text{l}$  deionized water droplets on the various film surfaces. Error bars are limiting values estimated from five measurements

Film description	Contact angle ( $^\circ$ )
PS film	$87.3 \pm 1.3$
Fullerene filled PS film ( $\phi_{\text{filler}} = 0.01$ )	$88.1 \pm 1.1$
Spin coated fullerene layer	$69.5 \pm 4.5$
Evaporated carbon layer	$65.5 \pm 1.0$

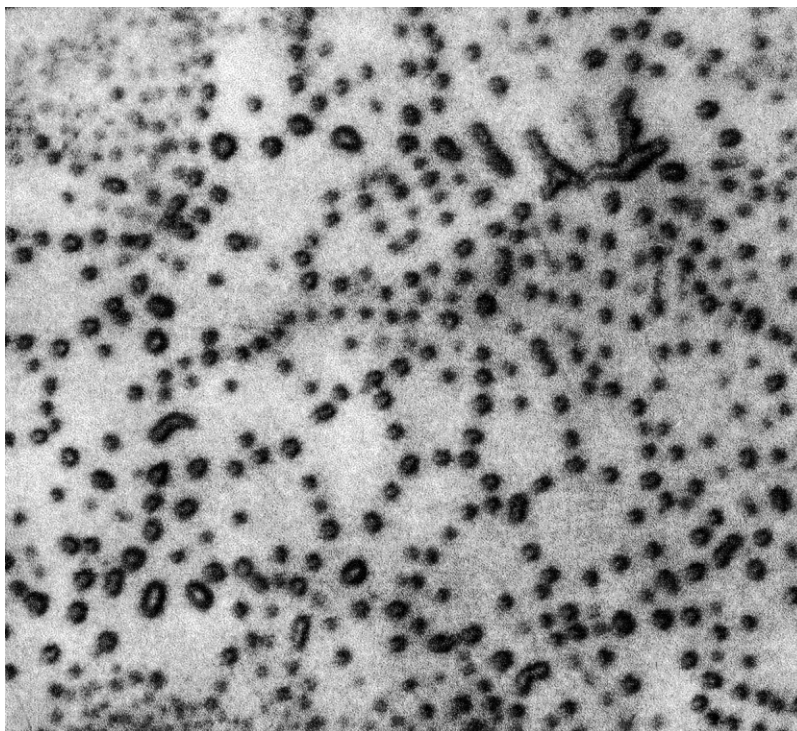


Fig. 8. Late-stage dewetting of a G0 PEOX film on a PS substrate at 135°C after 25 min. Due to small sample size, thickness of PEOX and PS layers are only estimated from solution concentrations and spinning speed to be in the range of 20–50 and 50–100 nm, respectively. Image width is 125  $\mu\text{m}$ . This dewetting pattern resembles observations of late stage dewetting in unentangled linear polymer films.

during growth (note the clover-leaf like shapes in Fig. 10). The shape distortions are similar to those found in (mathematical) two-dimensional soap bubbles where the distortions arise to minimize the surface perimeter, subject to constraints against coalescence [36–38]. These observations suggest that the highly branched (G2) hypergraft PEOX have a relatively large viscosity [39–40] that inhibits hole coalescence. Moreover, the present observations on G2 hypergraft PEOX suggest that these polymers might have similar viscoelastic properties to entangled polymer fluids.

Antonietti et al. [2,3,24] have recently pointed out that highly branched and nearly spherical nano-gel particles can exhibit bulk viscoelastic properties remarkably similar to melts of entangled linear polymers and Hempenius et al. [21] have noted a great similarity of the viscoelastic spectra of G2 hypergraft PS polymers to the ‘microgel’ particles of Antonietti et al. Gauthier et al. [41] have recently observed a tendency of G2 PS hypergraft molecules to form pearl-like chains of hypergraft molecules when Langmuir films of the dendrigraft polymer are spread

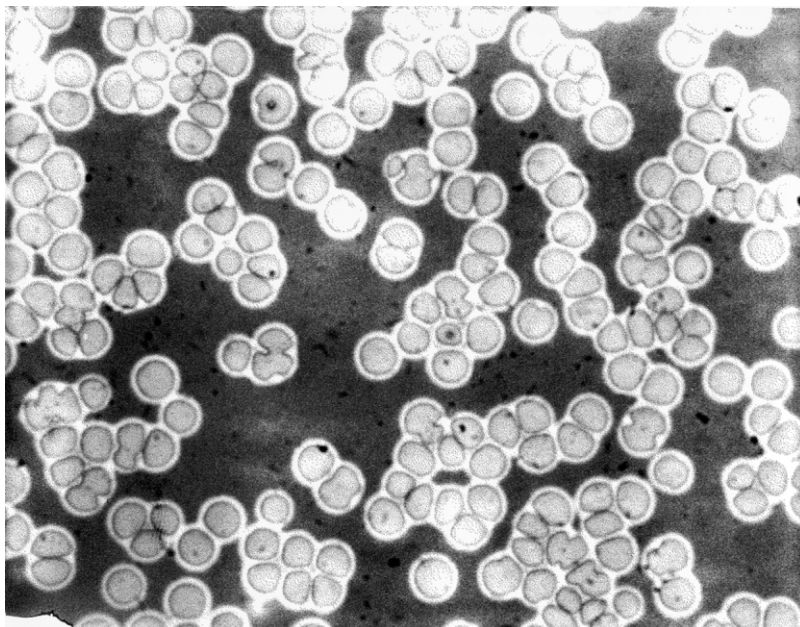


Fig. 9. Intermediate-stage dewetting of a G2 PEOX film in the 'hole-changing' regime. Film shown corresponds to an annealing time of 10 min at 130°C. Note the tendency of the holes formed in the early stage of dewetting (early stage not shown) to 'chain' and the inhibition against hole coalescence. Image width is 90  $\mu\text{m}$ .

onto water. This type of clustering is suggestive of equilibrium polymerization type particle clustering [42,43] in these highly branched polymers and this aggregation phenomenon could explain the viscoelastic properties of these branched molecule fluids<sup>7</sup>.

At a further later stage of the G2 PEOX dendrigraft film dewetting, the borders of the hole clusters begin to percolate and form a cellular network structure. Fig. 11 shows some of these cells as their boundaries begin to break up into droplets by a capillary instability. This signals the final droplet stage ( $t = 120$  min) of dewetting and the resulting droplet configuration for this G2 PEOX film is shown in Fig. 12. The film morphology seems to remain in the form of Fig. 12 upon further

---

<sup>7</sup> Douglas and Hubbard [Macromolecules 24, 3163 (1991)] have suggested a dynamic chain association model of chain entanglement based on the idea that collective chain motion in the form of equilibrium clusters occurs when the average chain dimensions becomes sufficiently large in comparison to their average chain cross-sectional diameter. An Onsager type condition for interparticle correlation then governs the 'entanglement' interaction in this model. Temperature is usually the control parameter for equilibrium polymerization so that temperature studies of the rheological properties of hyperbranched polymer fluids should be especially interesting [42,43].

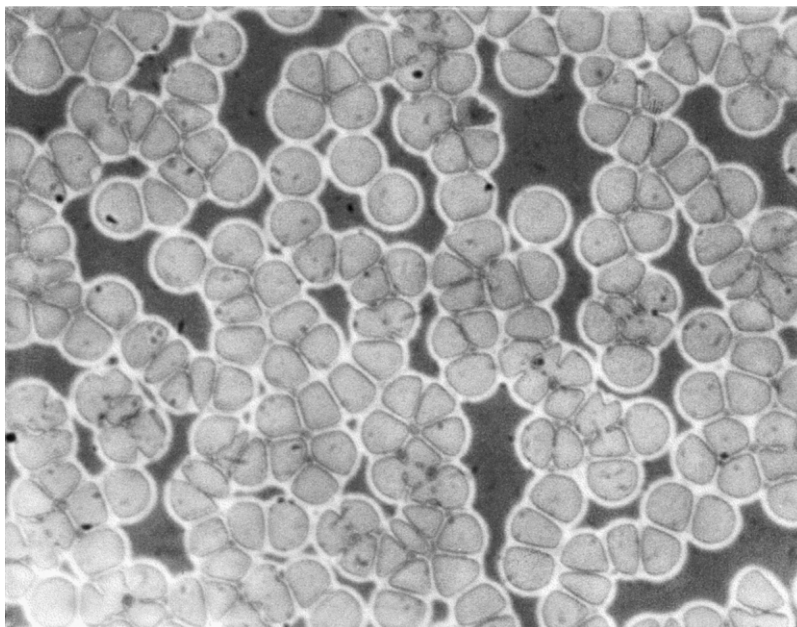


Fig. 10. Intermediate-stage dewetting of a G2 PEOX film in the ‘hole-distortion’ regime. Film shown corresponds to an annealing time of 15 min at 130°C. The holes continue to grow in size and impinge on each other, leading to hole shape distortion. Similar distortions of boundary shapes are seen in interacting soap bubbles [36,38]. Image width is 90  $\mu\text{m}$ .

annealing and no significant change in the shape or size of the droplets is seen even after a time  $t = 300$  min. Note the relatively uniform distribution (no pattern) of the droplet configuration in Fig. 12 (albeit more polydisperse droplet sizes), in comparison to G0 PEOX of Fig. 8. While substrate heterogeneity may play a role in droplet size polydispersity, we believe that film viscoelasticity differences between G0 and G2 have a large impact on the final morphology of the dewet film. A similar effect is found for a solid inorganic substrate, as discussed below.

In Fig. 13 we show the image of dewetting of G2 PEOX film from an acid cleaned silica wafer. This late-stage film dewetting pattern should be compared to the one found for the G2 PEOX film on polystyrene substrate in Fig. 12. We speculate that the pattern observed in Fig. 13 arises from an earlier fingering instability pattern (similar to those observed previously for high molecular weight PS on silanized silica [34]) which subsequently breaks up by capillary instability to give a ‘Floral’ droplet pattern. Fig. 14 shows the late-stage dewetting pattern of the G0 PEOX from the silica wafer as a control measurement that has a similar Voronoi pattern as for linear PS dewetting on Si shown in Fig. 4a. The dewetting pattern of the G0 film corresponds to conventional observations for late-stage dewetting. (Essentially the same results were also obtained for a linear chain

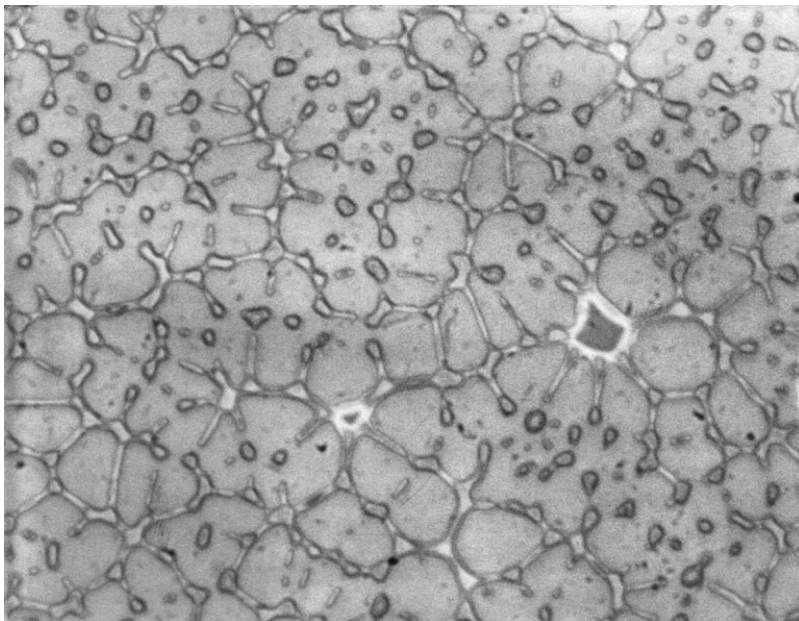


Fig. 11. Intermediate-stage dewetting of a G2 PEOX film in the 'froth' regime. Film shown corresponds to an annealing time of 45 min at 130°C. The connectivity of the hole clusters spans the entire systems forming a foam-like network ('froth'). Observe the relative uniformity of the cell size and shape and the widths of the fluid borders of the cells. Image width is 90  $\mu\text{m}$ .

PEOX film of molecular weight  $M_w = 30\,000$  g/mol and these results are not shown because of their similarity to the G0 films.) Thus, polymer branching (and presumably the associated change in film viscoelasticity) can have a significant influence on the dewetting morphology. The nature of the substrate whether polymeric or inorganic that affects the driving force for dewetting influences the late-stage dewet pattern morphology of the higher viscosity G2 film, but not of the G0 PEOX films. Changes in the rate of dewetting arising from the substrate chemistry can generally be anticipated since the driving force for dewetting depends on the surface energy.

#### 4. Conclusion

The addition of 'impurities' to polymer films is generally considered to have a detrimental effect on the film wetting properties. Indeed, small particles and air bubbles in polymer films have been found to cause film dewetting [19,20]. Heterogeneities on the film surface have also been implicated. The present paper shows that the addition of nanofiller particles to a spun-cast polymer film can actually

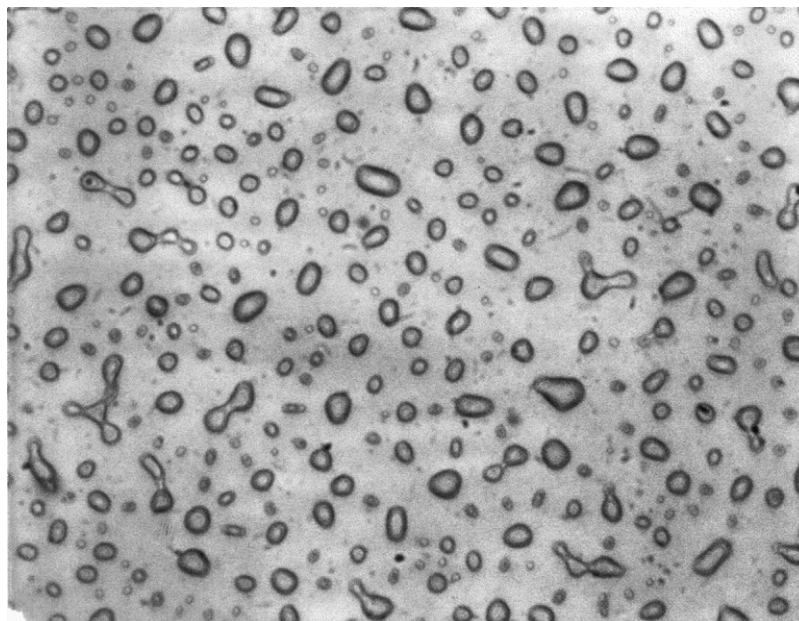


Fig. 12. Late-stage dewetting of a G2 PEOX film in the droplet regime. Film shown corresponds to an annealing time of 120 min at 130°C. Fluid cell borders shown in Fig. 11 break up into droplets. Note the relative uniformity of droplet size and coverage in comparison to the G0 film shown in Fig. 8. The break-up of the fluid cell borders is accompanied by a retraction of the liquid into droplets that lie near the cell vertices of the former hole ‘froth’. The droplet distribution does not appear to evolve significantly in the late stage of dewetting, apart from a tendency for the droplets to become increasingly circular. Image width is 90  $\mu\text{m}$ .

stabilize the film against dewetting. The evidence available suggests that the fullerenes segregate to the solid substrate and modify the polymer-surface interaction and geometry. The diffuseness of the adsorbed filler layer and the heterogeneity of the filler concentration within the plane of the layer are apparently important for understanding the observed film stabilization. A similar film stabilization effect has been seen in films cast on substrates roughened and chemically modified through irradiation [14,15]. Filled films appear to provide a different strategy for modifying the substrate geometry and chemistry. Regardless of the specific process or processes responsible for the stabilization observed in our measurements, the effect promises to be an important means of controlling thin polymer film dewetting for applications such as optical and electronic coatings, adhesion, sensors, etc. The evidence available suggests that the stabilization process may be an equilibrium phenomenon, making the method useful for achieving the long-term stabilization of polymer films and coatings.

We also investigated the influence of polymer branching (generation number G) on the dewetting of hypergraft poly(2-ethyl-2-oxazoline) (PEOX) polymer films

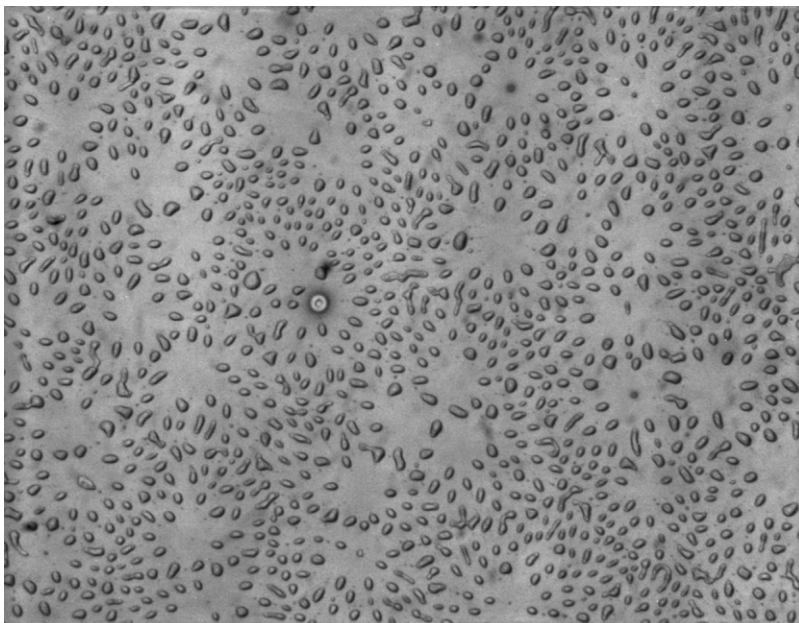


Fig. 13. Late-stage dewetting of a G2 PEOX film dewetting from an acid-cleaned silica substrate. Film was annealed at 120°C for 120 min. As in the case of the films on PS substrates, the G2 polymer films on acid-cleaned silica substrates form a relatively uniform distribution of droplets. However, note the presence of a large-scale correlation in the droplet dewetting patterns that we have informally termed ‘floral’ patterns. Kinetic studies of the dewetting process are required to check this interpretation of the floral patterns. Image width is 300  $\mu\text{m}$ .

from model non-polar synthetic polymer and inorganic substrates. The present study contrasts the cases of a zeroth generation G0 hypergraft, which is a comb polymer and a G2 hypergraft, which resembles a nearly spherical micro-gel particle. The early stage of dewetting is found to be similar in the G0 and G2 films and is largely independent of substrate (entangled polystyrene film or acid-cleaned silica wafer). However, the late stage of dewetting in the G2 films differs significantly from the G0 films because of an inhibition of hole coalescence in the intermediate stage of film dewetting. The holes in the G2 hyperbranched films continue to grow in size until they impinge on each other to form a foam-like structure with a uniform ‘cell’ size [44]. The boundaries of these cells break-up and the vertices of the former cellular network retract to form a uniformly distributed droplet configuration, in contrast to a floral cascading pattern on inorganic Si surface. In comparison, hole coalescence in the G0 films occurs readily resulting in a ‘Voronoi’ [45] droplet configuration that is normally associated with film dewetting of simple liquids on organic and inorganic surfaces. Similar trends have been observed in the dewetting of linear polymer films where entangled polymers

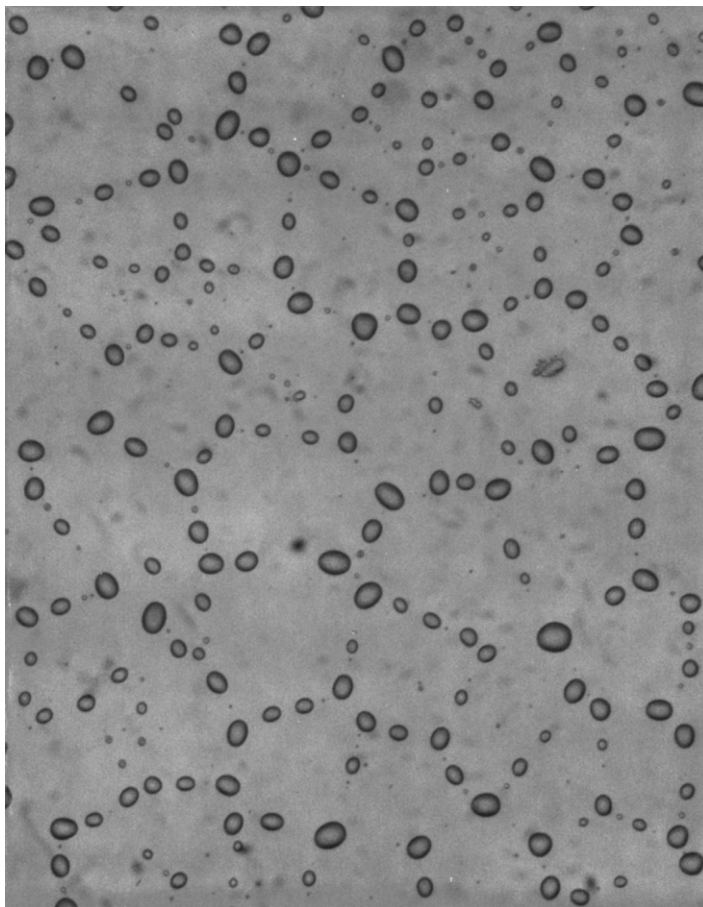


Fig. 14. Late-stage dewetting of a G0 PEOX film dewetting from an acid-cleaned silica substrate. Film was annealed at 120°C for 120 min. As in Fig. 8, a 'Voronoi tessellation' pattern [45] is found, reflecting the break-up of the hierarchical network structure formed through facile hole coalescence [44]. Image width is 300  $\mu\text{m}$ .

behave similarly to the branched (G2) polymers of the present study. These differences are attributed to the viscoelasticity of the G2 hyperbranched polymer.

### **Acknowledgements**

The authors would like to thank Dr Tinh Nguyen for assistance with contact angle measurements and Drs Sushil Satija, Holger Gruell and Alan Esker for assistance with the neutron reflectivity measurements. We thank Barry Bauer at

NIST and Dendritech Inc., Midland, MI for the PEOX samples used in the study and in particular Drs Rui Yin, Donald Tomalia, David Hedstrand and Douglas Swanson. This work is partially supported by the US Army Research Office under contract number 35109-CH.

## References

- [1] J.J. Lisari, *Plastic Coatings for Electronics*, McGraw-Hill, N.Y., 1970.
- [2] J.M.G. Cowie, *Polymer: Chemistry and Physics of Modern Materials*, Chapman and Hall, New York, 1970.
- [3] S. Wu, *Polymer Interfaces and Adhesion*, Marcel Dekker, New York, 1982.
- [4] G. Reiter, *Phys. Rev. Lett.* 68 (1992) 75.
- [5] G. Reiter, *Macromolecules* 27 (1993) 3046.
- [6] S. Herminghaus, K. Jacobs, K. Mecke, J. Bischof, A. Fery, M. Ibn-Elhaj, S. Schlagowski, *Science* 282 (1998) 916.
- [7] R. Xie, A. Karim, J.F. Douglas, C.C. Han, R.A. Weiss, *Phys. Rev. Lett.* 81 (1998) 1251.
- [8] J.C. Meredith, A.P. Smith, A. Karim, E.J. Amis, *Macromolecules* 33 (2000) 9747.
- [9] A. Vrij, *Disc. Farad. Soc.* 42 (1966) 23.
- [10] F. Brochard-Wyart, J. Dalliant, *Can. J. Phys.* 68 (1990) 1084.
- [11] Yerushalmi-Rozen, R., Klein, J., Fetters, L.J, *Science*, 263 (1994) 793, See ref. 34.
- [12] Y. Feng, A. Karim, R.A. Weiss, J.F. Douglas, C.C. Han, *Macromolecules* 31 (1998) 484.
- [13] G. Henn, D.G. Bucknall, M. Stamm, P. Vanhoorne, R. Jerome, *Macromolecules* 29 (1996) 4305.
- [14] T. Kerle, R. Yersushalmi-Rozen, J. Klein, L.J. Fetters, *Europhys. Lett.* 38 (1997) 207.
- [15] T. Kerle, R. Yersushalmi-Rozen, J. Klein, L.J. Fetters, *Europhys. Lett.* 44 (1998) 484.
- [16] K.A. Barnes, J.F. Douglas, A. Karim, D.-W. Liu, E.J. Amis, *Polym. Intern.* 49 (2000) 463.
- [17] F.J. Hahn, *J. Paint Technol.* 43 (1971) 58.
- [18] L.O. Kornum, H.K. R. Nielsen, *Prog. Organ. Coat.* 8 (1980) 275.
- [19] T.G. Stange, D.F. Evans, W.A. Hendrickson, *Langmuir* 13 (1997) 4459.
- [20] K. Jacobs, S. Herminghaus, K.R. Mecke, *Langmuir* 14 (1998) 965.
- [21] M.A. Hempenius, W.F. Zoetelief, M. Gauthier, M. Möller, *Macromolecules* 31 (1998) 2299.
- [22] J.D. Ferry, *Viscoelastic properties of Polymers*, Wiley, NewYork, 1980.
- [23] M. Antonietti, W. Bremsler, M. Schmidt, *Macromolecules* 23 (1990) 3796.
- [24] M. Antonietti, T. Pakula, W. Bremsler, *Macromolecules* 28 (1995) 4227.
- [25] T.P. Russell, A. Karim, A. Mansour, G.P. Felcher, *Macromolecules* 21 (1998) 1890.
- [26] J. Roovers, W.W. Graessley, *Macromolecules* 14 (1981) 766.
- [27] See ref. 19.
- [28] R. Yin, D.A. Tomalia, J. Kukowska-Latallo, J.R. Baker, *PMSE Preprints* 71 (1997) 206.
- [29] R.S. Frank, G. Merkle, M. Gauthier, *Macromolecules* 30 (1997) 5397.
- [30] S.S. Sheiko, M. Gauthier, M. Möller, *Macromolecules* 30 (1997) 2350.
- [31] I.V. Zolotukhin, L.I. Yanchenko, E.K. Belonogov, *JETP* 67 (1998) 720.
- [32] P. Brant, A. Karim, J.F. Douglas, F.S. Bates, *Macromolecules* 29 (1996) 5628.
- [33] T. Onda, S. Shibuichi, N. Satoh, K. Tsuji, *Langmuir* 12 (1996) 2125.
- [34] G. Reiter, *Langmuir* 9 (1993) 1344.
- [35] A. Faldi, R.J. Composto, K.I. Winey, *Langmuir* 11 (1995) 4855.
- [36] J. Foisy, M. Alfaro, J. Brock, N. Hodges, Z. Zimba, *Pacific J. Math.* 159 (1993) 47.
- [37] F. Morgan, *Pacific J. Math.* 165 (1994) 347.
- [38] F.J. Almgren Jr., J.E. Taylor, *Sci. Am.* 235 (1976) 82.
- [39] D.T. Wasan, J.J. Mc Namara, S.M. Shah, K. Sampath, *J. Rheol.* 23 (1979) 181.
- [40] A. Karim, J.F. Douglas, S.K. Satija, R.J. Goyette, C.C. Han, *Macromolecules* 32 (1999) 1119.

- [41] M. Gauthier, L. Cao, M.H. Rafailovitch, J. Sokolov, *Polymer Preprint* 40 (2) (1999) 114.
- [42] J. Dudowicz, K.F. Freed, J.F. Douglas, *J. Chem. Phys.* 111 (1999) 7116.
- [43] J. Dudowicz, K.F. Freed, J.F. Douglas, *J. Chem. Phys.* 112 (2000) 1002.
- [44] M.O. Magnasco, *Phil. Mag. B* 65 (1992) 895.
- [45] D. Weaire, N. Rivier, *Contemp. Phys.* 25 (1984) 59.